Selective hydrogenation of C=C bond over N-doped reduced graphene oxides supported Pd catalyst

Renfeng Nie [a,b], Meng Miao [a], Weichen Du [a], Juanjuan Shi [a], Yingchun Liu [a,*], Zhaoyin Hou [a,*]

[a] Department of Chemistry, Zhejiang University, Hangzhou 310028, PR China
[b] College of Chemistry & Chemical Engineering, Hubei University, Wuhan 430062, PR China

ARTICLE INFO

ABSTRACT

In this work, N-doped reduced graphene oxides (NRGO) was synthesized *via* a facile urea-hydrothermal treatment of graphene oxide and used as support for ultrafine Pd nanoparticles (NPs). It was found that N in NRGO can improve the dispersion of Pd NPs. NRGO supported Pd catalyst (Pd/NRGO) is highly active and selective for the hydrogenation of C=C bond in cinnamaldehyde and hydrogenation of phenol to cyclohexanone under mild conditions. X-ray diffraction, X-ray photoelectron spectra and transmission electron microscopy characterizations confirmed the interaction between NRGO and Pd enhanced with the amount of N atom in NRGO. Raman spectroscopy of adsorbed cinnamaldehyde on Pd/NRGO suggested that NRGO played a positive role in the selective activation of C=C bond in cinnamaldehyde.

© 2015 Elsevier B.V. All rights reserved.

1. Introduction

Selective activation of multiple carbon–carbon bonds and/or benzene ring is of great importance in chemical industry [1,2]. Among of which, hydrogenation of cinnamaldehyde is a popularly reported model reaction for the selective activation of α, β-unsaturated carbonyl compounds [3,4], selective hydrogenation of phenol to cyclohexanone is an important step in the production of Nylon 6, Nylon 66, and polyamide resins [5–7]. Up to now, selective activation and catalytic conversion of unsaturated carbon–carbon bonds to desired product over heterogenous catalyst with hydrogen is a challenge work [8]. In published works, a lot of stabilizer or surfacant-protected noble metals nanoparticles (NPs) and heterogenous materials supported noble metals NPs were reported for these reactions [9], while metal leach or agglomeration of NPs happens occasionally because of the weak anchorage of supports. At the same time, the strong absorption of stabilizers or surfacant around NPs often prohibits those very active surface atoms. In order to overcome these problems, several groups found Pd NPs, Ru NPs and Ir NPs that encapsulated in pores of microporous and mesoporous materials (zeolites, MOFs, carbon, etc.) exhibited higher stability and activity under mild conditions [6,10–14]. And it was recommended that those modified supports with element-incorporation (N, P, etc.) can control the growth and aggregation of NPs [15,16].

Recently, a newly one-atom-thick sheet of carbon–graphene has attracted attention of scientists all over the world. This two-dimensional material exhibits excellent thermal, mechanical and electrical properties, which make it promising for potential applications in catalysis [17–19]. More recently, many researchers reported that N-doped carbon nanostructures with *n*-type or metallic behavior have greater electron mobility than their pristine carbon nanostructures [20–24]. And N-doping can also introduce chemically active sites for catalytic reactions and anchoring sites for metal nanoparticle deposition, which may enable the applications of graphene with improved performance in catalysis.

In this work, we want to report a simple preparation method of N-doped reduced graphene oxides (NRGO) supported Pd NPs and its application in the selective activation of C=C bond and benzene ring under mild conditions. The role of N dopant for the dispersion of Pd on NRGO and the activation of cinnamaldehyde were discussed.

2. Experimental

2.1. Catalyst preparation

Graphene oxides (GO) was prepared *via* oxidation of graphite according to the Hummers and Offemann's method [25]. GO (81 mg) was first dispersed in 70 mL of deionized water, a given

* Corresponding authors. Fax: +86 571 88273283.
E-mail addresses: liuyingch@zju.edu.cn (Y. Liu), zyhou@zju.edu.cn (Z. Hou).

Table 1
Pd dispersion and elemental analysis of different catalysts.[a]

Catalyst	Mass concentration (%)					Particles size (nm)	
	C	O	N	Pd	Pd[b]	XRD	TEM
GO	62.5	37.5	–	–	–	–	–
RGO	80.8	19.2	–	–	–	–	–
NRGO$_{-150}$	84.4	13.2	2.4	–	–	–	–
NRGO$_{-300}$	79.9	12.6	7.5	–	–	–	–
Pd/RGO	78.1	17.2	–	4.7	4.5	11.1	15.7
Pd/GO	80.0	15.5	–	4.5	4.6	13.4	16.5
Pd/NRGO$_{-150}$	80.6	12.3	2.5	4.6	4.5	3.2	5.1
Pd/NRGO$_{-300}$	75.9	12.2	7.3	4.6	4.6	<1.4	1.6

[a] Mass concentrations were detected in XPS analysis, the value of mass concentration of Pd was the relative quantity to the mass of C.
[b] Mass concentration of Pd was detected *via* ICP, the value was the relative quantity to the mass of C.

amount of urea was added into the GO dispersion, and followed by sonication for 3 h. Above solution was then transferred into a 100 mL Teflon-lined autoclave and kept at 180 °C for 10 h. After urea-hydrothermal treatment, the product, denoted as NRGO$_{-x}$ (where x represents the weight ratio of urea/GO), was filtered, washed, and dried at 40 °C in vacuum oven for overnight. The synthesis procedure of reduced graphene oxide (RGO) was the same as NRGO$_{-x}$ without the addition of urea.

After that, graphene-based support (50 mg) was dispersed in water (43 mL), and a controlled amount of PdCl$_2$ was added to above suspension, followed by stirring for 0.5 h. And then, the suspension was reduced in a 100 mL Teflon-lined autoclave at 40 °C, 2 MPa H$_2$ for 8 h. The final composite, labeled as Pd/NRGO$_{-x}$ (or Pd/RGO and Pd/GO) was filtered and washed with deionized water until free of Cl$^-$ and finally dried in a vacuum oven at 40 °C for 10 h. The real amount of loading Pd was detected via inductively coupled plasma-atomic emission spectroscopy (ICP, Plasma-Spec-II spectrometer) and summarized in Table 1.

2.2. Characterization

X-ray diffraction (XRD) analysis were carried out on a RIGAKU D/MAX 2550/PC diffractometer at 40 kV and 100 mA with Cu Kα radiation (λ = 1.5406 Å) in the range from 5 to 80°. Surface composition of the pretreated samples was checked using an FT-IR spectroscopy (OPUS) in the range of 400–4000 cm^{-1}. Samples for IR characterizations were prepared by compressing a well-mixed 3 mg of catalysts powder with 200 mg of potassium bromide (KBr). X-ray photoelectron spectra (XPS) were recorded on a PerkinElmer PHI ESCA System. X-ray source was standard Mg anode (1253.6 eV) at 12 kV and 300 W. Transmission electron microscopy (TEM) images were obtained using an accelerating voltage of 200 kV (TEM, JEOL-135 2010F). Scanning transmission electron microscope and high-angle annular dark-field (STEM–HAADF) images were collected on FEI TECNAI G2 F30 S-TWIN (S)TEM operating

at 300 kV. Raman spectra were collected from 100 to 4000 cm^{-1} with 514.5-nm argon ion laser (Rhenishaw Instruments, England) at room temperature. The spectra were recorded with a resolution of 2 cm^{-1}.

2.3. Catalytic test

The hydrogenation reaction was carried out in a 25 mL custom designed stainless autoclave with a Teflon inner layer. In a typical procedure, a certain amount of catalyst was dispersed in 2.5 mL solvent, and then put into a controlled amount of substrate. The reactor was sealed, purged and pressurized with hydrogen. The reaction was stirred with a magnetic stirrer at a rate of 1000 rpm (MAG-NEO, RV-06 M, Japan) under predetermined temperature and time. After reaction, the mixture was separated by CCl$_4$ extraction and centrifugation in order to remove the water and solid catalyst (see Fig. S1 in Supporting information). The reactants were analysed by gas-chromatogram (GC, HP 5890, USA) with a 30 m capillary column (HP-5) using a flame ionization detector. And all products were confirmed by GC–MS (Agilent 6890) as well as by comparing the retention times to respective standards in GC traces.

3. Results and discussion

3.1. Characterizations

3.1.1. XRD

Fig. 1 presents the XRD patterns of prepared supports and Pd-based catalysts. The obvious shift of C(0 0 2) peak from 10.8 (in GO) to nearly 25° (in RGO and NRGO$_{-300}$) was observed in XRD patterns of graphene-based supports (Fig. 1a), which indicates that GO was reduced by partially removing surface oxygen-containing groups (see Table 1) and then restacked to a poorly ordered graphite-like material [26,27]. The (0 0 2) peak of NRGO$_{-300}$ is weaker and boarder than that of RGO, which could be attributed to
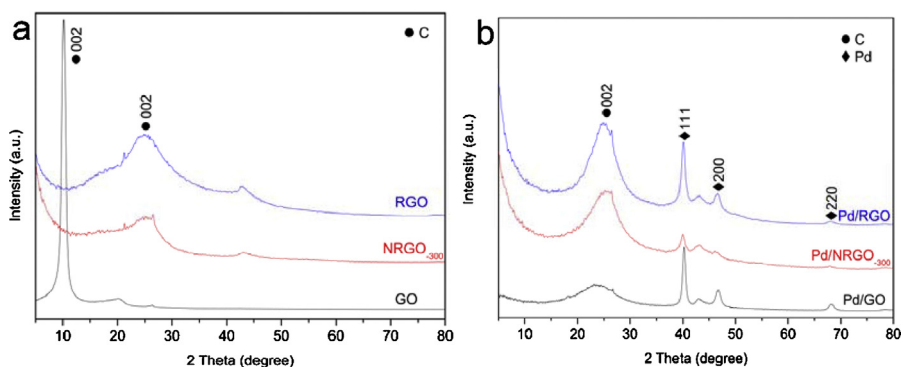

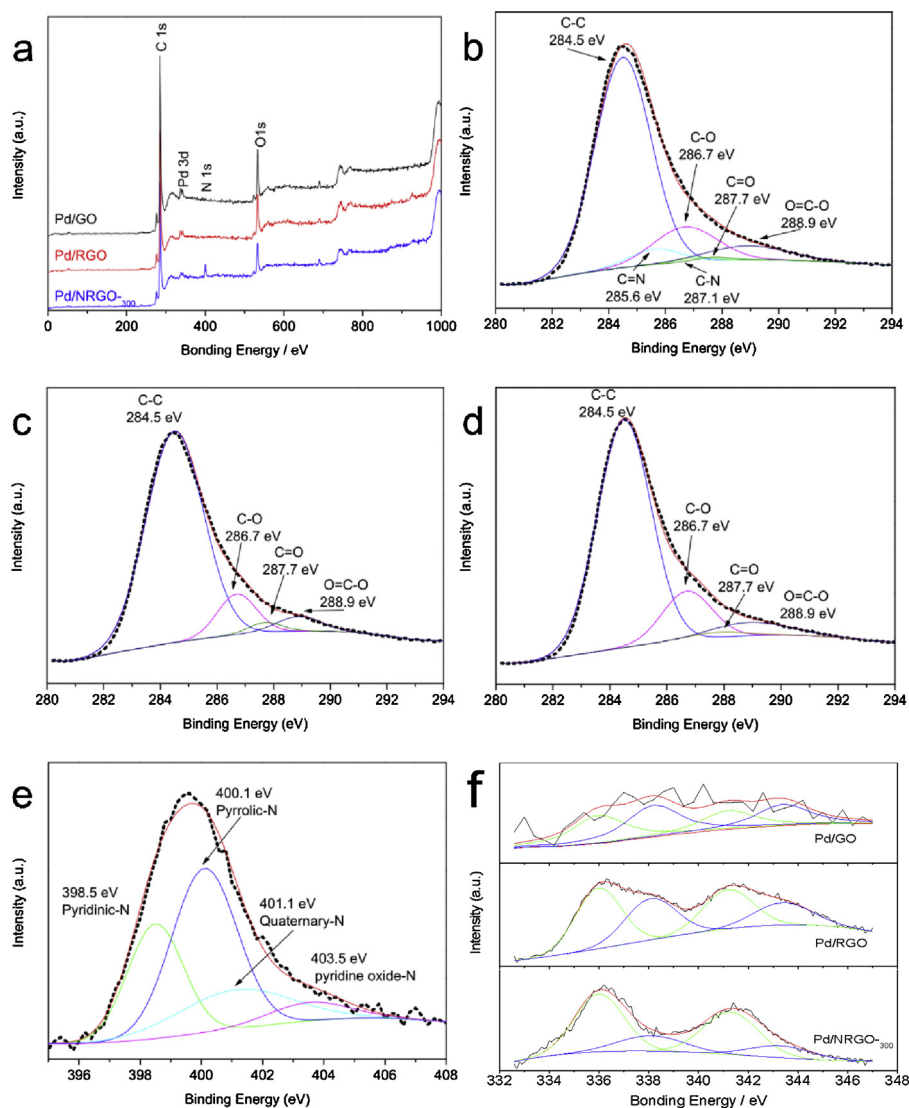**Fig. 1.** XRD patterns of (a) supports and (b) Pd-based catalysts.

Fig. 2. (a) XPS survey spectra, C1s spectra in (b) Pd/NRGO$_{-300}$, (c) Pd/RGO and (d) Pd/GO, (e) N1s spectrum of Pd/NRGO$_{-300}$, (f) Pd2p spectra of Pd/NRGO$_{-300}$, Pd/RGO and Pd/GO.

less re-graphitization of NRGO$_{300}$ because of the incorporation of nitrogen atoms into carbon skeletal of graphene. These results indicated that the re-graphitization of graphene sheets in RGO could be partially depressed by N-dopant in NRGO. Fig. 1b presents the XRD patterns of these carbon materials supported Pd catalysts prepared by mild H$_2$ reduction. The small broad peak around 23.5° (0.37 nm) in Pd/GO indicated that GO can also be reduced during the PdCl$_2$ reduction process (40 °C, 2 MPa H$_2$ for 8 h) [28]. The location of C (002) peak (at 25.1°) remains stable when Pd were loaded on RGO or NRGO$_{-300}$ supports. Pd/NRGO$_{-300}$ showed a broader diffraction peak of Pd, in which peaks at 40.0, 46.6 and 68.4° in the XRD pattern fit well with the characteristic (1 1 1), (2 0 0) and (2 2 0) planes of Pd NPs, respectively [29,30]. According to Scherrer's formula and the half-width of (1 1 1) peak, the calculated size of Pd crystallites in Pd/NRGO$_{-300}$ is 1.4 nm (Table 1), which is smaller than that of Pd/GO (13.4 nm) and Pd/RGO (11.1 nm). These results indicated that N-dopant in NRGO$_{-300}$ can improve the dispersion of Pd.

3.1.2. FT-IR

In order to gain further insights on the chemical changes caused by urea-hydrothermal reduction, FT-IR spectroscopic measurements were performed and shown in Fig. S2. The vibrational peaks of pristine GO are consistent with the presence of fingerprint groups such as carboxylic species, hydroxyl species and epoxy species (O—H stretch, 3418 cm^{-1}; C=O stretching vibration, 1720 cm^{-1}; O—H bending of absorbed water, 1628 cm^{-1}; OH deformation, 1385 cm^{-1}; C—OH stretching, 1228 cm^{-1}; alkoxy C—O stretch, 1091 cm^{-1}) [31,32]. After non-urea hydrothermal treatment, the FT-IR spectrum of RGO shows weak C=O peak in addition to a board O—H stretching band, along with a significant weaken for C—OH stretching. These results inferred that a fraction of O—H and C=O groups distributed over the carbon basal plane disappeared after hydrothermal treatment [33,34]. The FT-IR spectrum of NRGO$_{-300}$ shows a unique sharp peak of C—O stretching at 1091 cm^{-1} exclusively from alkoxy C—O stretch as well as the sp^2 C=N and/or C=C at 1559 cm^{-1}, along with the C—C and/or C—N stretching at 1456 cm^{-1} [33]. Above results confirmed that oxygen species in GO disappeared and N was introduced into the framework of graphene during the urea-hydrothermal pretreatment (see Table 1).

3.1.3. XPS analysis

Fig. 2 shows XPS spectra of graphene-based hybrids. It can be found that high percentage of oxygen-containing groups
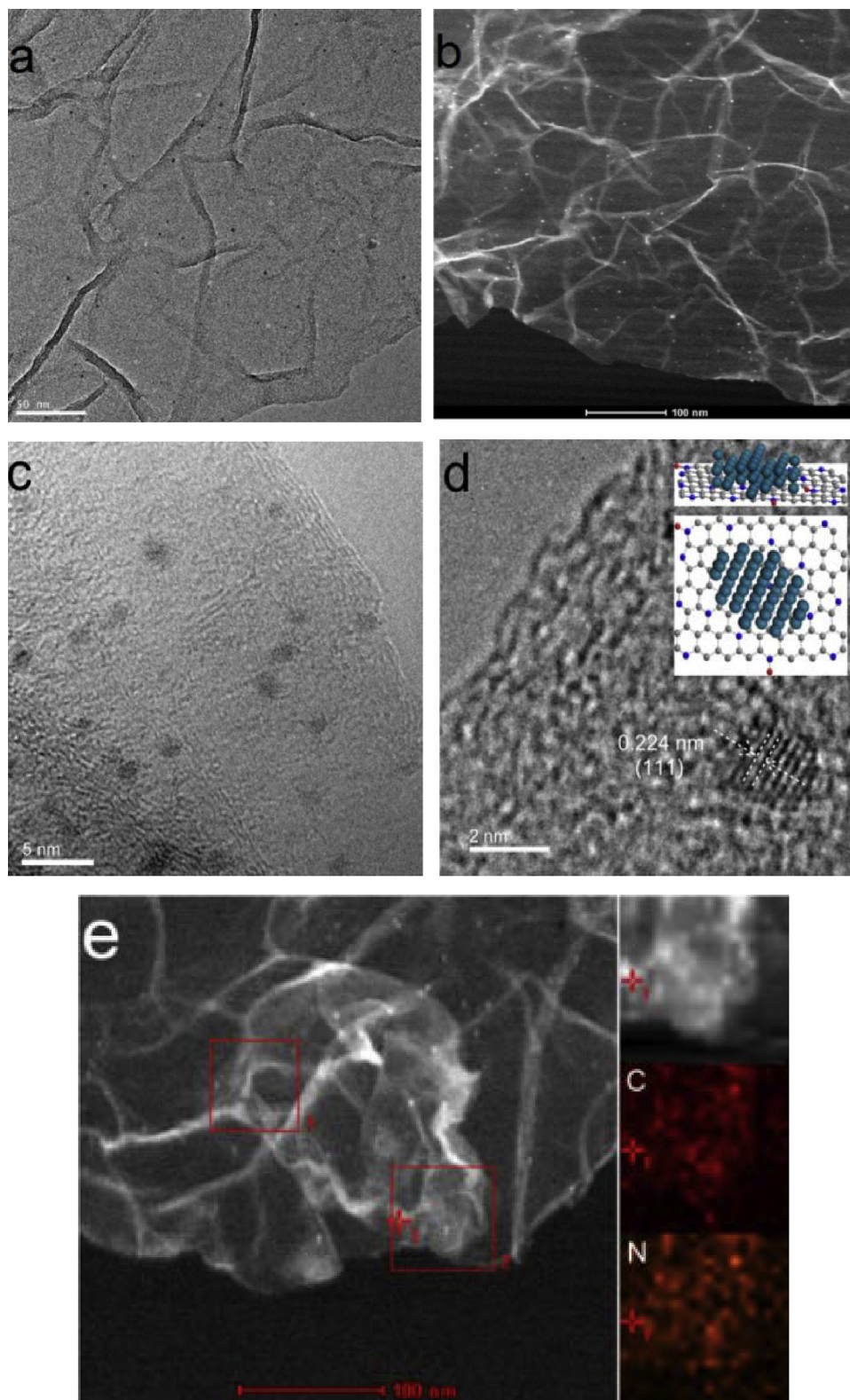
Fig. 3. (a, c and d) TEM and (b and e) HAADF–STEM images of fresh Pd/NRGO$_{-300}$.

disappeared in NRGO$_{-300}$ and RGO compared with GO, especially in the form of C—O and C≡O (Table S1). After the loading of Pd NPs under mild H$_2$ atmosphere, the amount of oxygen was further decreased due to catalytic reduction of Pd NPs via H$_2$-support-Pd ternary redox system (Fig. 2b–d) [35]. Deconvolution of the C1s peak in Pd/NRGO$_{-300}$ (Fig. 2b) reveals the presence of 5.7%

carbon–nitrogen bonds at 285.6 and 287.1 eV, which are attributed to sp^2 C—N and sp^3 C—N bonds, respectively [20–22]. The high-resolution N 1s spectrum of the Pd/NRGO$_{-300}$ (Fig. 2e) confirms the presence of graphitic, pyridinic, pyrrolic, and pyridine oxide like N atoms [36]. These results, once again, confirmed the successful intercalation of N atoms into the graphene skeleton by the
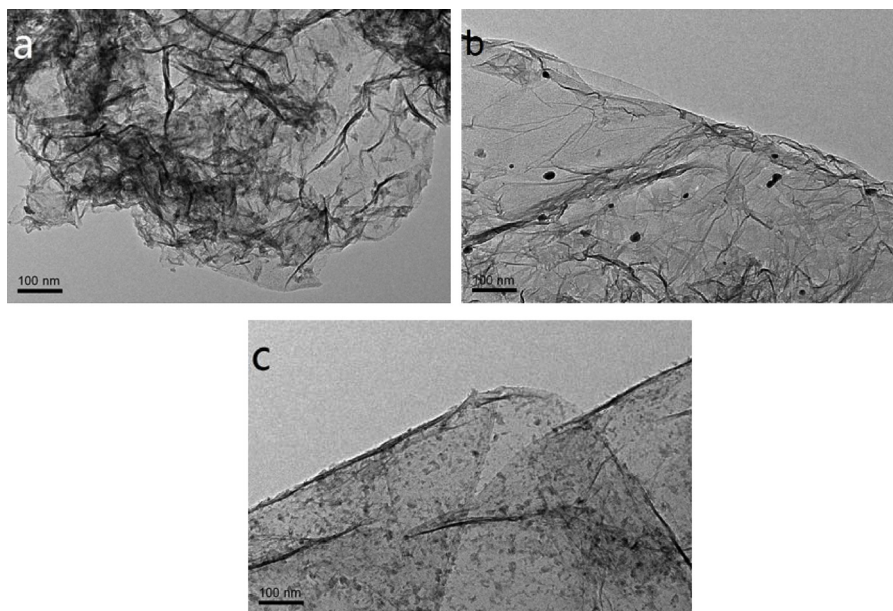
Fig. 4. TEM images of (a) Pd/NRGO$_{-150}$, (b) Pd/RGO, and (c) Pd/GO.

hydrothermal treatment between GO and urea. XPS analysis also revealed that Pd-3d$_{5/2}$ binding energy in Pd/NRGO$_{-300}$ contained more metallic Pd (75% Pd^0) than that of N-free Pd/RGO (59%) and Pd/GO (47%) (Fig. 2f), which can be attributed to the strong electron donating effect of NRGO [37].

3.1.4. TEM

Fig. 3 presents the TEM and STEM images of Pd/NRGO$_{-300}$ with different magnifications. It can be seen that Pd NPs with a mean diameter of 1.6 nm are fairly well dispersed on the thin graphene layers (Fig. 3a), and it was well consistent with STEM observations (Fig. 3b). High resolution TEM images (Fig. 3c and d) reveal the well crystallized (1 1 1) face of Pd NPs with a lattice space of 0.224 nm. As observed in elemental maps and linescans of Pd/NRGO$_{-300}$ (Figs. 3e, and S3), there is a good spatial correspondence of C and N elemental maps formed with the intensities of their K lines, indicating that N doping formed homogeneously over the entire graphene sheets. As reference, the mean sizes of the Pd NPs supported on NRGO$_{-150}$, RGO and GO are found to be 5.1, 15.7 and 16.5 nm, respectively (Fig. 4). These results further confirmed that N species in NRGO can improve the dispersion Pd nanoparticles.

3.2. Selective activation of carbon–carbon bond

At first, hydrogenation of cinnamaldehyde (CALD) over these carbon materials supported Pd catalysts were carried out as a model reaction and these results were summarized in Table 2. It can be found that Pd/NRGO$_{-300}$ gives higher activity (82.5%, entry 1) and higher selectivity toward hydrocinnamyl dehyde (HALD) (95.9%) than that of commercial Pd/C (entry 6). In a control experiment, NRGO$_{-150}$ (with 2.1% N content) supported Pd catalyst exhibits a lower activity (51.5%) than Pd/NRGO$_{-300}$, while the selectivity toward HALD remains as high as 93.4%. On the other hand, N-free catalysts (Pd/RGO and Pd/GO) are difficult to catalyze this reaction along with a significant decrease in HALD selectivity under the same condition. At the same time, it was found that HALD is stable in this system, as further prolongation in reaction time to 8 h produces a deeper hydrogenation product with only 24.5% yield (entry 7). This might be ascribed to the interaction between C=O group and N species on support, which uniquely protects the C=O group away from Pd, thus inhibits further hydrogenation of HALD
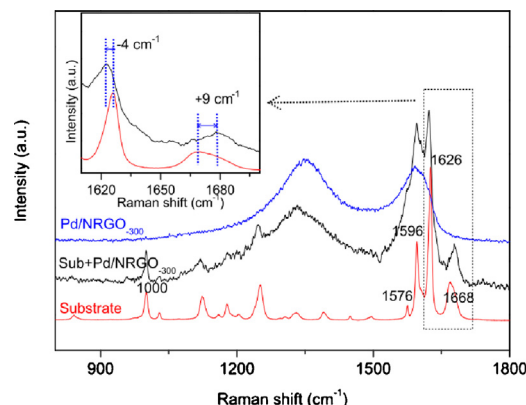
Fig. 5. Raman study of the interaction between Pd/NRGO$_{-300}$ and CALD.

(Fig. S4). And it is also interesting to find that water was favorable for the separation of Pd/NRGO$_{-300}$ (see Fig. S1), and the conversion of CALD is higher when water was added in the reaction mixture (see Table S2), which might be attributed to that water can enhance the polarization of CALD and prevent the side reactions of CALD.

In order to better understand the high selectivity toward C=C bond over NRGO supported Pd catalyst, the interaction between adsorbed CALD and Pd/NRGO$_{-300}$ was checked *via* Raman spectroscopy (Fig. 5). Pd/NRGO$_{-300}$ was added into a mixture containing of 2.5 mL ethyl acetate and 10 mmol CALD under vigorous stirring at 70 °C for 1 h. Then, catalyst in the mixture was separated by centrifugation, and dry at room temperature for overnight before Raman analysis. It was found that the vibration frequency of ν (C=C) band at 1626 cm^{-1} decreases to 1622 cm^{-1}, while the vibration of ν (C=O) band at 1668 cm^{-1} shifts to 1675 cm^{-1} (Fig. 5). These results indicate that N species in the skeleton of graphene are expected to anchor −CHO group of CALD, followed by the obvious blueshift of ν (C=O) band. That is, the incorporated nitrogen in graphene plays a crucial role for selective hydrogenation of CALD (Fig. S4).

Besides the ease of separation of heterogeneous catalysts, their recycle is also an important issue for the development of sustainable chemical. The Pd/NRGO$_{-300}$ catalyst can be reused for several cycles without obvious losing in its activity (Fig. S5).

Table 2
Hydrogenation of cinnamaldehyde over different catalysts.[a]

Entry	Catalysts	t (h)	Conv. (%)	Selectivity (%)		
				Hydrocinnamal dehyde	Cinnamyl alcohol	Hydrocinnamal alcohol
1	Pd/NRGO$_{-300}$	0.5	82.5	95.9	0	4.1
2	Pd/NRGO$_{-300}$	0.75	99.6	96.1	0	3.9
3	Pd/NRGO$_{-150}$	0.5	51.5	93.4	0	6.6
4	Pd/RGO	0.5	9.0	87.3	0	12.7
5	Pd/GO	0.5	8.8	86.4	0	13.6
6	Pd/C[b]	0.5	50.3	84.7	0	15.3
7	Pd/NRGO$_{-300}$	8	>99.9	75.5	0	24.5
8[c]	Pd/NRGO$_{-300}$	1.75	>99.9	96.5	0	3.5
9[d]	Pd/NRGO$_{-300}$	1.75	90.1	94.3	0	5.7
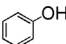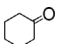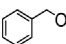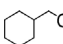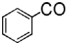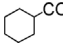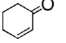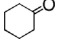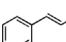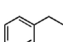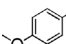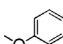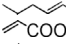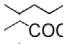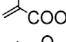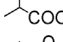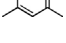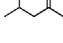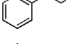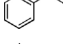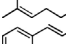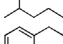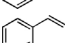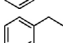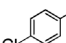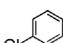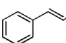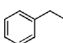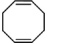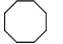
[a] Reaction conditions: 2 mmol CALD, catalyst (0.01 mol% Pd), 2.5 mL H_2O, 70 °C, 2 MPa H_2.
[b] Purchased from Aladdin Chemistry Co., Ltd.
[c] 10 mmol CALD, catalyst (0.002 mol% Pd).
[d] Fifth run to test the reusability of catalyst under the conditions of entry 8.

Table 3
Selective hydrogenation of unsaturated hydrocarbons over Pd/NRGO$_{-300}$.[a]

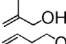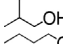| Entry	Substrates	Selectivity (%)	Conv. (%)	T (°C)	t (h)
1[b]		>99	41.3	30	8
2[b]		98.9	98.8	30	24
3[b]		97.4	94.0	50	13
4[b]		95.2	94.6	90	3
5[c]		86.8	>99	90	3
6[c]		>99	93.7	70	4.5
7		>99	>99	70	0.8
8[d]		>99	>99	70	0.5
9		98	>99	70	0.5
10		81.5	21.6	70	0.5
11		70.6	50.7	70	2
12		99.2	>99	70	0.5
13		>99	>99	70	0.5
14		>99	>99	70	0.5
15[e]		>99	97.3	70	1
16[d]		>99	97.5	70	1
17[d]		>99	95.6	70	1
18		>99	>99	70	1
19[d]		>99	>99	70	0.5
20[d]		>99	>99	70	0.5
21[d]		>99	>99	70	0.5
22[d]		94.1	>99	70	0.5
23[d]		>99	98.6	70	2
24[e]		>99	>99	70	1
25[e]		>99	>99	70	1

[a] Reaction conditions: substrate (2 mmol), catalyst (0.01 mol% Pd), H_2O (2.5 mL), H_2 (2 MPa).
[b] Substrate (0.1 mmol), catalyst (2.1 mol%), H_2 (0.2 MPa).
[c] Substrate (0.3 mmol), catalyst (0.7 mol%), H_2 (3 MPa).
[d] Substrate (1 mmol), catalyst (0.02 mol%).
[e] Substrate (0.5 mmol), catalyst (0.04 mol%).

Selective hydrogenation toward different unsaturated substrates was also investigated in order to demonstrate the versatility of Pd/NRGO$_{-300}$ catalyst (see Table 3). Because of the great importance of cyclohexanone [10], selective hydrogenation of phenol to cyclohexanone was carried out at first. The conversion of phenol reached 41.3% with a cyclohexanone selectivity exceeding 99% within 8 h at 0.2 MPa and 30 °C (entry 1), and further increased up to 98.8% with a 98.9% selectivity at 24 h (entry 2).

At higher temperature (50 °C), the conversion of phenol achieved 94% with a 97.4% selectivity within 13 h (entry 3); further increase in temperature (to 90 °C) shortened the reaction time (3 h), but slightly reduced the selectivity of cyclohexanone (95.2%) (entry 4). Next, a more challenging hydrogenation of benzyl alcohol toward cyclohexane-methanol, due to the competitive hydrogenation and hydrogenolysis, was demonstrated and the result was shown in entry 5. Under 3 MPa of H_2, full conversion of benzyl alcohol was obtained in 3 h at 90 °C with a selectivity of 86.8%. Other substituted aromatic compounds, such as benzoic acid, afforded the corresponding cyclohexane–carboxylic acid in a good yield (entry 6). Pd/NRGO$-_{300}$ could be considered in a sense as a universal catalyst for the CC double bond hydrogenation of various function groups, including aldehydes, ketones, alcohols, acids, esters etc. Most of the reactants were converted to the corresponding reduced products in excellent yields within 1 h. Among olefins studied, in general, α, β-unsaturated aldehydes, acids, esters as well as aromatic olefins were found to be more reactive compared to ketones and alcohols. In the case of aliphatic olefins, such as citral, Pd/NRGO-$_{300}$ was less active and only moderate product yield was achieved in longer reaction times, probably as a result of two C=C bonds, electron-donating function as well as steric constraint in the same molecular.

4. Conclusions

It was found that NRGO was especially adapted for anchoring very fine ($\sim$1.6 nm) Pd NPs due to the enhanced interaction between Pd and N in NRGO. This NRGO supported Pd catalyst can selectively catalyze the hydrogenation of C=C or benzene ring when other easily reducible groups, such as hydroxyls and carbonyls, are present. At the same time, Raman analysis of adsorbed CALD indicated that N species in the skeleton of graphene can also anchor —CHO group of CALD and make C=C bond in the same molecular activated.

Acknowledgements

Appendix A. Supplementary data

Supplementary data associated with this article can be found, in the online version, at http://dx.doi.org/10.1016/j.apcatb.2015.07.015

References

[1] C.H. Jun, Chem. Soc. Rev. 33 (2004) 610–618.
[2] Y. Yamamoto, U. Radhakrishnan, Chem. Soc. Rev. 28 (1999) 199–207.
[3] N. Morimoto, S. Yamamoto, Y. Takeuchi, Y. Nishina, RSC Adv. 3 (2013) 15608–15612.
[4] F. Zhao, Y. Ikushima, M. Chatterjee, M. Shirai, M. Arai, Green Chem. 5 (2003) 76–79.
[5] A. Dimian, C. Bildea, Front Matter, Wiley Online Library, 2008.
[6] H. Liu, Y. Li, R. Luque, H. Jiang, Adv. Synth. Catal. 353 (2011) 3107–3113.
[7] K. Mori, S. Furubayashi, Chem. Commun. 48 (2012).
[8] A. Corma, Science 313 (2006) 332–334.
[9] G. Kyriakou, M.B. Boucher, A.D. Jewell, E.A. Lewis, T.J. Lawton, A.E. Baber, H.L. Tierney, M. Flytzani-Stephanopoulos, E.C.H. Sykes, Science 335 (2012) 1209–1212.
[10] H. Liu, T. Jiang, B. Han, S. Liang, Y. Zhou, Science 326 (2009) 1250–1252.
[11] X. Yang, D. Chen, S. Liao, H. Song, Y. Li, Z. Fu, J. Catal. 291 (2012) 36–43.
[12] L. Shang, T. Bian, B. Zhang, D. Zhang, L.Z. Wu, C.H. Tung, Angew. Chem. Int. Ed. 126 (2014) 254–258.
[13] M. Yurderi, A. Bulut, M. Zahmakiran, M. Gülcan, S. Özkar, Appl. Catal. B 160–161 (2014) 534–541.
[14] Y. Tonbul, M. Zahmakiran, S. Özkar, Appl. Catal. B 148–149 (2014) 466–472.
[15] X. Zhao, J. Zhu, L. Liang, C. Li, C. Liu, J. Liao, W. Xing, Appl. Catal. B 154–155 (2014) 177–182.
[16] M. Latorre-Sánchez, A. Primo, H. García, Angew. Chem. Int. Ed. 52 (2013) 11813–11816.
[17] G.E. Antolini, Appl. Catal. B 123–124 (2012) 52–68.
[18] A.R. Siamaki, A.E.R.S. Khder, V. Abdelsayed, M.S. El-Shall, B.F. Gupton, J. Catal. 279 (2011) 1–11.
[19] Y. Gao, D. Ma, C. Wang, J. Guan, X. Bao, Chem. Commun. 47 (2011) 2432–2434.
[20] Y. Liang, Y. Li, H. Wang, J. Zhou, J. Wang, T. Regier, Nat. Mater. 10 (2011) 780–786.
[21] X. Wang, X. Cao, L. Bourgeois, H. Guan, S. Chen, Y. Zhong, Adv. Funct. Mater. 22 (2012) 2682–2690.
[22] Y. Li, Y. Zhao, H. Cheng, Y. Hu, G. Shi, L. Dai, J. Am. Chem. Soc. 134 (2012) 15–18.
[23] R. Saada, S. Kellici, T. Heil, D. Morgan, B. Saha, Appl. Catal. B 168–169 (2015) 353–362.
[24] C.H. Choi, M.W. Chung, H.C. Kwon, J.H. Chung, S.I. Woo, Appl. Catal. B 144 (2014) 760–766.
[25] W.S. Hummers, R.E. Offeman, J. Am. Chem. Soc. 80 (1958) 1339.
[26] R. Nie, J. Wang, L. Wang, Y. Qin, P. Chen, Z. Hou, Carbon 50 (2012) 586–596.
[27] R. Nie, J. Shi, W. Du, W. Ning, Z. Hou, F. Xiao, J. Mater. Chem. A 1 (2013) 9037–9045.
[28] X. Chen, G. Wu, J. Chen, X. Chen, Z. Xie, X. Wang, J. Am. Chem. Soc. 133 (2011) 3693–3695.
[29] G. Wu, X. Wang, N. Guan, L. Li, Appl. Catal. B 136–137 (2013) 177–185.
[30] D. Teschner, J. Borsodi, A. Wootsch, Z. Revay, M. Havecker, A. Knop-Gericke, S. David Jackson, R. Schlogl, Science 320 (2008) 86–89.
[31] V.H. Pham, T.V. Cuong, S.H. Hur, E. Oh, E.J. Kim, E.W. Shin, J. Mater. Chem. 21 (2011) 3371–3377.
[32] M. Jahan, Q. Bao, K.P. Loh, J. Am. Chem. Soc. 134 (2012) 6707–6713.
[33] T. Van Khai, H.G. Na, D.S. Kwak, Y.J. Kwon, H. Ham, K.B. Shim, Carbon 50 (2012) 3799–3806.
[34] K.J. Huang, D.J. Niu, J.Y. Sun, C.H. Han, Z.W. Wu, Y.L. Li, Colloid Surf. B 82 (2011) 543–549.
[35] R. Nie, J. Shi, W. Du, Z. Hou, Appl. Catal. A 473 (2014) 1–6.
[36] R. Arrigo, M. Hävecker, R. Schlögl, D.S. Su, Chem. Commun. (2008) 4891–4893.
[37] H. Li, L. Liu, S. Xie, M. Qiao, W. Dai, Y. Liu, Adv. Funct. Mater. 18 (2008) 3235–3241.